# The accomplices: Heparan sulfates and N-glycans foster SARS-CoV-2 spike:ACE2 receptor binding and virus priming

Giulia Paiardi [1,2,3,8,] *, Matheus Ferraz [3,4,5], Marco Rusnati [6], Rebecca C. Wade [1,2,3,7,] *

[1] Heidelberg University, Heidelberg, Germany
[2] Zentrum für Molekulare Biologie (ZMBH), DKFZ-ZMBH-Alliance, Heidelberg University, Heidelberg, Germany
[3]Molecular and Cellular Modeling Group, Heidelberg Institute for Theoretical Studies (HITS), Heidelberg, Germany
[4] Department of Virology, Aggeu Magalhães Institute, Oswaldo Cruz Foundation, FIOCRUZ, Recife, PE, Brazil
[5] Department of Fundamental Chemistry, Federal University of Pernambuco, UFPE, Recife, PE, Brazil
[6] Macromolecular Interaction Analysis Unit, Section of Experimental Oncology and Immunology, Department of Molecular and Translational Medicine, Brescia, Italy
[7] Interdisciplinary Center for Scientific Computing (IWR), Heidelberg University, Heidelberg, Germany
[8] Lead contact

* Correspondence: giulia.paiardi@h-its.org; rebecca.wade@h-its.org.

**Summary**

The SARS-CoV-2 spike glycoprotein mediates virus attachment to human host cells by binding angiotensin-converting enzyme 2 (ACE2) and heparan sulfate (HS) proteoglycans. To elucidate the structure, dynamics, and functional consequences of these interactions, we carried out microsecond-long all-atom molecular dynamics simulations, followed by random acceleration molecular dynamics simulations, of the fully glycosylated spike:ACE2 complex with and without heparin chains bound. We find that heparin, a model for HS, promotes structural and energetic stabilization of the active conformation of the spike receptor binding domain (RBD) and reorientation of ACE2 toward the N-terminal domain in the same spike subunit as the RBD. Spike and ACE2 N-glycans exert synergistic effects, promoting better packing, strengthening the protein:protein interaction, and prolonging the residence time of the complex. ACE2 and heparin binding trigger rearrangement of the S2' functional site through allosteric interdomain communication. HS thus has a multifaceted role in facilitating SARS-CoV-2 infection.

*Keywords*: SARS-CoV-2, spike, N-glycan, heparan sulfate, heparin, ACE2 receptor, molecular dynamics simulation, glycoprotein interactions, protein allostery, conformational dynamics.

## Introduction

Despite the clinical success of vaccines, the continued emergence of SARS-CoV-2 variants highlights the need for a deeper understanding of the infection mechanisms for developing better therapeutics for treating COVID-19. The SARS-CoV-2 viral surface spike glycoprotein (spike) is a type I membrane glycoprotein that exists as a homotrimer on the virion surface and mediates the initial steps of infection. Each subunit ($S_A$, $S_B$, $S_C$) of the prefusion spike is composed of two regions, S1 and S2. S1, containing the N-terminal domain (NTD) and the receptor binding domain (RBD), wraps around S2, which forms a central helical bundle with two heptad repeats and contains the fusion peptide (FP) (Lan et al., 2020; Walls et al., 2020; Wang et al., 2020; Yuan et al., 2020). 66 N-glycans are covalently attached to the protein

surface of the trimeric spike ectodomain (Grant et al., 2020; Watanabe et al., 2020; Xie & Butler, 2023; Zhao et al., 2020). Beyond generally shielding the protein surface, these N-glycans have been found to control spike activation, modulate the protein:protein interactions, and sterically mask functional epitopes of the viral protein (Casalino et al., 2020; Harbison et al., 2022; Mori et al., 2021; Nangarlia et al., 2023; Newby et al., 2023; Sztain et al., 2021; Q. Yang et al., 2020). The prefusion spike has been shown to adopt inactive closed and active open conformations (Walls et al., 2020). In the open, active conformation, the RBD is exposed so that its receptor binding motif (RBm) can interact with the human angiotensin-converting enzyme 2 (ACE2) receptor (Hoffmann et al., 2020; Shin et al., 2022; J. Yang et al., 2020). The interaction with ACE2 triggers the priming of spike, which entails the cleavage of the S2' functional site by the human transmembrane serine protease 2 (TMPRSS2) (Vankadari et al., 2022; Yu et al., 2022), the subsequent shedding of S1, and the conformational rearrangement of S2, propelling the FP into the target membrane and initiating membrane fusion (Dodero-Rojas et al., 2021; Essalmani et al., 2022).

Heparan sulfate (HS) proteoglycans (HSPGs) are expressed on the surface of human cells. They are composed of a core protein with covalently attached long, variably sulfated polysaccharide chains. HSPGs are co-receptors for SARS-CoV-2 infection and bind spike via its basic domains (Clausen et al., 2020; Kim et al., 2020; Liu et al., 2021; Sun et al., 2023). The variability of sulfation patterns in HS across different individuals, tissues, and cell types may contribute to virus tropism, although this variability hinders a full comprehension of their mechanistic role (Kearns et al., 2022). Heparin, a long, linear, highly-sulfated polyanionic oligomer, is frequently used as a model for HS in experimental studies due to their structural similarity (Hogwood et al., 2023). Computational and experimental studies have demonstrated that heparin can act as a potent antiviral agent by competing with HSPGs for binding to spike (Clausen et al., 2020; Kim et al., 2022; Kim et al., 2020; Liu et al., 2021; Mycroft-West et al., 2020; Paiardi et al., 2022; Sun et al., 2023; Tree et al., 2021) and, intriguingly, that spike forms a ternary complex by simultaneously binding ACE2 and heparin or HS (Cecon et al., 2022; Clausen et al., 2020; Kim et al., 2023). We previously characterized the anti-viral effects of heparin on SARS-CoV-2 by performing over 20µs of all-atom molecular dynamics (MD) simulation of spike in closed and open conformations, each with zero, one or three heparin chains bound. The long heparin chains bound in a basic groove on spike and spanned from the basic domain on the RBD of one subunit to the S1/S2 basic domain of the preceding subunit (Paiardi et al., 2022). Our simulations indicated that heparin binding hindered the opening of closed spike, while allowing the binding of ACE2 to the open conformation of S, as observed in experimental studies (Cecon et al., 2022; Clausen et al., 2020; Kim et al., 2023).

A comprehensive understanding of the dynamics governing the process of SARS-CoV-2 priming upon ACE2 engagement, as well as the roles of N-glycans and HS, has so far evaded experimental characterization, making MD simulations the method of choice for investigating these mechanisms. Therefore, we performed ten 1-µs all-atom conventional MD simulations followed by a total of over 300 ns of random acceleration molecular dynamics (RAMD) to investigate how the interaction between SARS-CoV-2 (Wuhan variant) prefusion spike in the active conformation and human ACE2-RBD (hereafter referred to as ACE2) is affected by heparin binding. For interpreting these simulations, we consider heparin as a model for HS due to its structural similarities. We also investigate the effect of N-glycans on the structural dynamics and allosteric force transmission between ACE2 and spike upon human receptor engagement.

## Results and Discussion

**Heparin stabilizes the open-spike:ACE2 RBD complex by direct and indirect interactions.**

We performed replica all-atom conventional MD simulations to generate representative ensembles of equilibrium complexes of the spike:ACE2 complex with and without heparin bound (Fig.1). The initial structural models of the fully glycosylated open spike ectodomain without heparin bound and with three heparin chains bound were obtained from (Paiardi et al., 2022). ACE2 was added by superimposition from the crystal structure of the ACE2-RBD:spike-RBD complex (Lan et al., 2020). In the models, ACE2 binds to the up-RBD of the $S_C$ subunit of the open spike homotrimer in both the presence and absence of three heparin chains (Fig.1). Each simulated system consisted of almost 1 million atoms (see STAR Methods for details).

The open spike:ACE2 complex, both with and without the heparin chains, remained structurally stable during all the conventional MD simulations with no dissociation noticeable by visual inspection. The computed root mean squared deviation (RMSD) confirms the convergence of the systems, which were reasonably equilibrated after 200ns (Fig. S1A). Overall, the systems with heparin equilibrated faster than those without heparin and they were more stable along the trajectories. The RMSD values of the systems show an overall lower deviation for $S_C$ in the presence of heparin, most likely due to its direct interaction with heparin. Accordingly, the root mean squared fluctuation (RMSF) shows a lower fluctuation of the $S_C$ NTD and RBD in the presence of heparin (Fig. S1B-C), suggesting a stabilizing effect of the heparin chains on the spike:ACE2 interaction.

The heparin chains maintained stable H-bond interactions mainly with residues in the basic domains of spike (Tab. 1). The heparin1 and heparin3 chains each interact with the down-RBD of one subunit, the NTD and the S1/S2 site on the adjacent subunit and with N-glycans of both subunits (Fig. 1, Tab. 1 and Fig. S2). Heparin2 shares the same binding mode although it interacts with the up-RBD ($S_C$ RBD). Intriguingly, the first monosaccharides of heparin2 bound to the up-RBD interact tightly with the ACE2 N53 glycan, suggesting a potential stabilizing role, see next sections (Fig. 1, Tab. 1 and Fig. S2).

The computed average molecular mechanics-generalized Born surface area (MM/GBSA) binding free energy ($\Delta G_{bind}$) between spike and ACE2 over the last 100 ns of the simulations is -105.9 ± 5.8 kcal/mol in the absence of heparin and -123.2 ± 37.0 kcal/mol when heparin is bound (Tab. 2), indicating that heparin binding energetically stabilizes the spike:ACE2 complex. Importantly, the strong electrostatic repulsion between heparin and ACE2, which are both negatively charged, is countered by favorable van der Waals interactions, primarily with the N-glycans, which result in the greater energetic stability of the glycoprotein complex.

Overall, the atomic-detail model of the open spike:ACE2:heparin complex is consistent with surface plasmon resonance and mass photometry data, supporting the ability of the open spike to simultaneously bind to ACE2 and heparin or HS (Cecon et al., 2022; Clausen et al., 2020; Kim et al., 2023). Furthermore, these simulations underscore the ability of a single spike bound to ACE2 to accommodate up to 3 heparin chains. Based on the structural similarities between heparin and HS, the data support the hypothesis that at the cell surface, HS orchestrates the initial step of cellular attachment by latching onto spike and bringing the virus close to the epithelial cell membrane while exposing the spike RBm and thus promoting encounter with ACE2 and the formation of the ternary spike:ACE2:HS complex.

**Heparin enhances the open spike RBD:ACE2 interactions and cross-correlation motion.**

In the context of SARS-CoV-2 infection, it is necessary to consider all the possible strategies exploited by the virus to optimize the interaction with the host cell receptor. As the simulations show that heparin stabilizes the protein:protein complex, we investigated the effect of heparin binding at the $S_C$ RBm:ACE2 interface. At the interface between $S_C$ RBm and ACE2 in the absence of heparin, residue-residue interactions observed in crystal structures are well-maintained during the trajectories, as shown by H-bond analysis and computed contact occupancies (Fig. S3-4) (Tab. S1). The presence of heparin results in the loss of the polar interaction between $S_C$ N501 and ACE2 Y41 (Fig. 2A), which is not compensated by the formation of interactions with the polysaccharide (Fig. S2). However, heparin binding leads to the formation of new polar contacts between ACE2 and the spike $S_C$ RBm (D355-G502; K353-Y495; H34-S497; S19-G476, respectively) (Fig. 2B, Figs. S3-4, Tab. S1), thereby strengthening the protein:protein interaction.

To investigate the dynamically coupled motion of the complex and how it is affected by the heparin chains, Dynamic Cross-Correlation Matrices were computed for the $S_C$ RBm and ACE2 (Fig.2C, Fig.S5). Heparin binding increases the correlated movement of the $S_C$ RBm L3-loop (residues 472-490) with the ACE2 $\alpha$15-helix (residues 324-330) and β1-strand (residues 354-357) (Fig. 2A-inset, 2C and Fig. S6). In agreement, the RMSF of the $S_C$ RBD and L3-loop, which is known to be highly flexible (Spinello et al., 2020; Williams et al., 2022), is lower when heparin is bound, confirming the stabilizing effect exerted by the heparin chains (Fig. S7). Notably, Verkhivker and co-workers (Verkhivker et al., 2023) identified a negative cross-correlated movement of these residues in the newer omicron spike variants upon ACE2 binding in the absence of heparin, while Kim and colleagues (Kim et al., 2023) showed that omicron spike interactions with HS and ACE2 are significantly enhanced compared to the Wuhan variant. Consistent with these and our findings, newer omicron spike variants could require HS to stabilize the protein:protein interface for subsequent steps in the infection process.

In summary, the observed energetics and dynamics of the spike RBD and ACE2 indicate that heparin has a stabilizing effect on the open spike:ACE2 complex due to the gain of new interactions at the protein:protein interface and the increased coupling of the movement of the highly flexible L3-loop of $S_C$ RBD with the $\alpha$15-helix and β1-strand residues of ACE2. Newer omicron spike variants could exploit the same mechanism. The structural similarity between heparin and HS implies that, at the cell surface, the formation of a spike:ACE2:HS complex might stabilize the spike:ACE2 interface.

**Heparin energetically stabilizes the reorientation of ACE2 towards the spike-NTD.**

To investigate the ability of heparin to promote rearrangements beyond the $S_C$ RBm:ACE2 interface, the RMSD and RMSF of ACE2 (Fig. S1) and orientational vectors between ACE2 and spike were monitored along the trajectories (Fig. 3). The structure of ACE2 is well preserved in simulations with and without heparin (Fig. S1). However, the distance ***d*** between the center of mass (COM) of ACE2 and the COM of $S_C$ NTD is reduced upon heparin binding (Fig. 3A,B). The $\alpha$ and $\beta$ angles, defining the positions of ACE2 and the $S_C$ NTD with respect to the long axis of the spike homotrimer (Fig. 3A), show a narrower distribution upon heparin binding, suggesting that ACE2 has more freedom to reorient on spike in the absence of heparin and is constrained in a well-defined location upon binding the polysaccharide (Fig.3C and 3D). Overall, the data point to a putative involvement of the $S_C$ NTD in the $S_C$ RBD:ACE2

interaction, in agreement with a recent report highlighting that mutations in the hypervariable NTD regions increase protein-mediated fusion and cell entry (Qing et al., 2021).

To further investigate the role of the $S_C$ NTD, essential dynamics (ED) analysis of the $S_C$ subunit and ACE2 in the complexes with and without heparin was performed. Projection of $S_C$:ACE2 dynamics onto the first eigenvector (the vector with the largest variance in the trajectory) shows that, in the absence of heparin, the motion of ACE2 and $S_C$ NTD is randomly oriented (Fig. 3E and S8), in agreement with cryo-EM data of Xu and colleagues (Xu et al., 2021). In contrast, upon heparin binding, $S_C$:ACE2 dynamics along the first eigenvector indicate the reorientation of ACE2 and the $S_C$ NTD towards each other, in agreement with the reduced distance between their COMs (Fig. 3F and S8), indicating that the spike NTD and heparin may together contribute to the increased affinity of SARS-CoV-2 to ACE2.

To quantify the contribution of the $S_C$ NTD to ACE2 binding, the binding free energy of the system was decomposed by calculating the MM/GBSA interaction energy of ACE2 with the $S_C$ RBD versus the $S_C$ RBD+NTD both in the absence and presence of heparin. The average $\Delta G_{bind}$ between $S_C$ RBD and ACE2 is -70.0 ± 3.0 kcal/mol and -49.2 ± 13.1 kcal/mol in the absence and presence of heparin, respectively (Tab.2). Heparin binding thus has an unfavorable effect on the spike RBD:ACE2 complex, in line with measurements from native mass spectrometry coupled to gas-phase ion chemistry (Y. Yang et al., 2020), likely due to electrostatic repulsion between the strongly anionic heparin and the negatively charged ACE2. $S_C$ NTD does not significantly affect the $\Delta G_{bind}$ in the absence of heparin, with an average $\Delta G_{bind}$ of -72.3 ± 10.8 kcal/mol (Tab.2). Conversely, the $S_C$ NTD significantly contributes to the interaction energy with ACE2 in the presence of heparin, resulting in an average $\Delta G_{bind}$ of -86.0 ± 34.9 kcal/mol. Notably, this $S_C$ RBD+NTD:ACE2 interaction energy is almost 70% of the binding free energy calculated for the simulated full-length spike (Tab.2).

Summarizing, the binding of heparin - and possibly HS - results in closer interactions between ACE2 and the $S_C$ NTD, reducing the orientational motion of ACE2 bound to spike, and driving the reorientation of ACE2 toward the $S_C$ NTD. Notably, site-directed mutagenesis and cell assays demonstrated that the NTD allosterically modulates spike-mediated functions, including TMPRSS2-dependent viral entry and fusogenicity (Meng et al., 2022; Qing et al., 2021; Qing et al., 2022)

**N-glycans of spike and ACE2 concur with heparin in strengthening the open spike:ACE2 interactions and extending the residence time of the complex.**

Genetic approaches and inhibition assays using the alkaloid kifunensine have demonstrated that blocking spike N-glycan biosynthesis significantly reduced spike:ACE2 binding (by 40%) and dramatically reduced (>95%) viral entry into ACE2-expressing cells (Q. Yang et al., 2020).

To assess the ability of N-glycans to stabilize the complex, the MM/GBSA $S_C$ RBD+NTD:ACE2 interaction energies were decomposed to compute the individual contributions of the protein and the N-glycans (Tab. 2). Interestingly, both with and without heparin, only half of the total interaction energy comes from protein:protein interactions, while the remaining half is due to glycans. Notably, the same trend is observed for the van der Waals term of the MM/GBSA interaction energy (Tab. 2), indicating that a key role of the N-glycans in stabilizing the spike:ACE2 complex is to fill intermolecular space and make favorable packing interactions. In addition, the buffering effect between the $S_C$ NTD and ACE2 is due to a dense H-bond network (Fig. S9). In the absence of heparin, H-bonds are mainly established by $S_C$ N17, N165 and N343 glycans simultaneously interacting with ACE2 N546

glycan and by spike $S_C$ N343 interacting with ACE2 N322 glycan (Fig. S9). Heparin binding promotes the interaction of $S_C$ N17 with ACE2 N322 and of $S_C$ N165 with ACE2 N90 and N322 glycans and with multiple residues of ACE2 (Fig. 4A and S9). Intriguingly, independently of the presence of heparin, the ACE2 N90 glycan inserts in the pocket between the back of the $S_C$ RBD (up-RBD) and $S_A$ RBD (Fig. 4A). In the absence of heparin, the ACE2 N90 glycan interacts with residues of $S_A$ and $S_C$ RBDs and $S_C$ N165 glycan (Fig. S9). Heparin binding strengthens the interaction between ACE2 N90 glycan and $S_A$ RBD residues by increasing the occupancy of the H-bonds and introducing further contacts ($S_A$ V445, $S_A$ S494). Interactions with $S_C$ RBD residues are overall maintained with the occupancy of some interactions reduced in favour of others, including the newly gained H-bond with $S_C$ G416 and the increased interaction with $S_C$ N165 glycan (Fig.4A and S9). These results provide a mechanistic explanation for previous reports of the importance of the N17, N165 and N343 glycans of spike and the N53, N90 and N322 glycans of ACE2 for their interaction (Hsu et al., 2023; Huang et al., 2021; Li et al., 2020; Mehdipour & Hummer, 2021; Q. Yang et al., 2020), by showing that spike and ACE2 N-glycans establish stable contacts and fill the intermolecular space, promoting more favorable protein:protein interactions. No experimental data are available concerning interactions of heparin or HS with N-glycans, making the model a potential starting point for further investigations.

To further investigate the mechanistic role of the N-glycans and heparin, the dissociation of ACE2 from spike was investigated by performing RAMD simulations following the τRAMD protocol (Kokh et al., 2018; Kokh et al., 2020). Although the large size of the simulated systems (see STAR Methods for details) meant that fully statistically converged RAMD residence times could not be calculated, the computed RAMD residence times of the spike:ACE2 complex without and with heparin chains bound of 2.2±0.2 and 3.1±1.2 ns, respectively, (Fig. S10) point to the stabilizing effect of the heparin chains that results in increased affinity and residence time of the complex, in line with TR-FRET measurements (Cecon et al., 2022). Visual inspection and analysis of the dissociation pathways unveiled the mechanisms by which N-glycans and heparin prolong the residence time. Dissociation of ACE2 in absence of heparin is in line with results from pulling MDs described by Zhu and coworkers (Zhu et al., 2022). Upon heparin binding, ACE2 follows the same dissociation path as without heparin, visiting multiple intermediate states, although the dissociation is slower (Fig.4B and Fig.S11-12):

1. In the first intermediate state, interactions between the buffering N-glycans at the interface between the $S_C$ NTD (N165, N17, N343) and ACE2 (N322, N546) are disrupted while conserving interactions between the $S_C$ RBm and ACE2-RBm (Fig. 4B, Fig. S11-12).
2. In the second intermediate state, the protein:protein dissociation evolves with a fan-like movement of ACE2, starting with the loss of polar interactions between L1-loop and L4-loop of spike and the respective interactors on the α1 helix of ACE2. Interactions between spike RBD L3-loop and the distal residues of the ACE2 N-terminus are still present (Fig. 4B, Fig. S11-12).
3. In the third and last intermediate state, contacts between the spike RBD L3-loop and the distal portion of ACE2 are lost, subsequently inducing the loss of interactions between ACE2 N90 glycan and the $S_C$ RBD until ACE2 is completely detached following an upward sliding movement (Fig. 4B, Fig. S11-12).

The second intermediate state is visited for a longer period in the presence of heparin due to direct interactions between the ACE2 N53 glycan and heparin2 (Fig. 4B, Fig. S9,11,12). Similarly, in the third intermediate state, the longer dissociation time in the presence of

heparin is due to stronger interactions established between the ACE2 N90 glycan and the spike RBDs, that result in a narrower crevice where the N-glycan is inserted (Fig. S9, S13).

Overall, when comparing the simulations with and without heparin, all the data point to the ability of the N-glycans and heparin to synergistically concur in extending the residence time of the open spike:ACE2 complex, supporting the hypothesis that N-glycans and HS may contribute to strengthening the spike:ACE2 interaction and packing.

**Allosteric communication pathways induced by ACE2 binding and modulated by heparin regulate rearrangement of the spike-TMPRSS2 site.**

The pronounced change in the dynamics of the systems upon ACE2 and heparin binding suggest that the binding partners not only affect spike residues at their immediate binding site but also induce long-range effects within spike. To reveal the residues and interactions specifically altered by the binding of ACE2 and heparin, Force Distribution Analysis (FDA) (Costescu & Gräter, 2013) was carried out by calculating the differences in the residue-based pairwise forces in the (i) open spike with and without ACE2 bound; (ii) open spike with ACE2 bound and with and without heparin bound. Fig. 5*A* shows the connected networks of residue pairs that exhibit changes in pairwise forces that exceed a given threshold. Changes in the force distribution pattern extend through the RBD domain of the $S_C$ subunit (bound to ACE2) to the $S_A$ RBD, from where the forces further propagate through the central helices of the $S_A$ and $S_B$ subunits, to the S1/S2 multifunctional domain and furin cleavage site of $S_B$ and the TMPRSS2 cleavage site of $S_A$. Represented as edges of the networks, N-glycans are only marginally involved in the propagation of the forces and are only visible upon application of a high pairwise force threshold (Fig. 5*A*).

To further explore the perturbation and potential allosteric effects on the prefusion spike, the changes in the time-averaged punctual stresses on each residue upon ACE2 binding to spike and upon heparin binding to the spike:ACE2 complex were computed. Notable differences in punctual stress were identified upon ACE2 or ACE2 and heparin engagement at residues within the NTD, RBD and central helices of spike even though none of these residues was in direct contact with ACE2 or heparin (Fig. S14,S15). Visual inspection, H-bond and accessible surface analysis of residues in the spike NTD and RBD did not show significant differences (data not shown), suggesting that the stress differences are driven by long-range electrostatic interactions between the negatively charged ACE2 or heparin and the charged residues of spike in proximity to the binding partners.

Particularly important for the intermolecular allostery upon either ACE2 or heparin binding are the residues located in the distal region of the central helices of each spike subunit (Fig. S14,S15), which have been suggested to have a stabilizing role on the S2 region in the spike prefusion conformation (Hsieh et al., 2020; Lu et al., 2022). Visual inspection and computation of H-bond occupancies revealed a bifurcated salt-bridge network between $S_A$ E773, $S_A$ R1019 and $S_B$ E1017 in spike (Fig. 5B). Upon ACE2 binding, the $S_A$ E773 - $S_A$ R1019 interaction becomes more transient (Fig. S16), while upon ACE2 and heparin binding, the occupancy of the $S_A$ E773 - $S_A$ R1019 H-bond decreases in favor of $S_A$ R1019 – $S_B$ E1017 (Fig. 5C,D), suggesting that heparin concurs in destabilizing the packing of the central helices and triggering subsequent rearrangements. Interestingly, another important residue for the intermolecular allostery upon ACE2 binding located in proximity to $S_A$ E773 is $S_A$ R815 (Fig. 5E and Fig. S14), the target of TMPRSS2 cleavage (Vankadari et al., 2022), which has been shown to be allosterically modulated by the spike NTD in infection and cell-cell fusion assays with chimeric spikes mutated in the NTD (Meng et al., 2022; Qing et al., 2021; Qing et al., 2022).

Visual inspection of $S_A$ R815 and computation of H-bond occupancies revealed that it forms previously unrecognized salt bridges with $S_A$ D839 and $S_A$ D843 of the adjacent intrinsically disordered FP, that were disrupted upon ACE2 or ACE2 and heparin binding (Fig. 5E,F). These observations are in line with increased exposure of $S_A$ R815 upon binding of ACE2 and binding of ACE2 and heparin (Fig. 5G). This provides an explanation of how R815 becomes available for priming by the TMPRSS2 protease, or alternatively for the binding of specific antibodies directed to this site only upon ACE2 binding (Essalmani et al., 2022; Low et al., 2022; Yu et al., 2022). No punctual stress or H-bonding rearrangement was recorded for R815 of $S_B$ and $S_C$ upon ACE2 binding (Fig. S14), suggesting that priming of the S1 portion and the subsequent rearrangement of the FP portion is propagated from the up-RBD of the subunit bound to ACE2 via the NTD and central helices to the S2' of the adjacent spike subunit. The reduced bonding cohesion between the interacting residues in the central helices increases the flexibility of the proximal loop containing R815, triggering the disruption of H-bonding and the subsequent exposition of the S2' cleavage site.

The $S_B$ N657 glycan, which is proximal to $S_A$ R815, was the only glycan identified as an additional punctual stress site upon either ACE2 or heparin binding (Fig. S17). Interestingly, site-directed mutagenesis demonstrated that the N657Q/D point mutation increased infectivity for reasons not yet clarified (Nangarlia et al., 2023; Yang et al., 2022). Visual inspection and H-bond analysis show that the N657 glycan gains interactions with D843 solely upon ACE2 binding (Fig. S18), and therefore when the residue loses its interactions with $S_A$ R815. The simulations suggest that upon ACE2 binding, the N657 glycan interacts with D843, possibly slowing down the exposition and rearrangement of the spike FP, explaining the increased infectivity of the virus after mutation. Furthermore, heparin binding induces loss of interactions between N657 glycan and D843, promoting the sequestering of the N657 glycan via allosteric effects due to the lack of direct interactions (Fig. S2 and S18), and thereby supporting spike infection by unmasking the spike FP and making it available for subsequent rearrangements.

In conclusion, ACE2 and HS directly promote viral infection by making spike accessible to cleavage by the human cell-surface proteases, which then leads to the activation of the viral protein. The spike and ACE2 N-glycans do not play a significant role in the propagation of the forces through spike upon ACE2 or heparin binding.

## CONCLUDING DISCUSSION

The infection mechanism of SARS-CoV-2 and the role of HS in priming virus attachment to the host cell receptor ACE2, initiating viral cell entry, has been studied by a range of experimental approaches (Clausen et al., 2020; Hoffmann et al., 2020; Kim et al., 2023; Kim et al., 2020; Liu et al., 2021; Mycroft-West et al., 2020; Shin et al., 2022; Tree et al., 2021; J. Yang et al., 2020; Y. Yang et al., 2020). Surface plasmon resonance and mass photometry showed the formation of a ternary spike:ACE2:heparin/HS complex (Cecon et al., 2022; Clausen et al., 2020; Kim et al., 2023). Nevertheless, the atomic detail structure and dynamics of the ternary spike:ACE2:HS complex have so far evaded experimental characterization, leaving open questions regarding the mechanistic role of the HS co-receptor in SARS-CoV-2 infection.

Here, we adopted a three-pronged strategy to address this gap. First, by performing microsecond-long conventional MD simulations of the spike:ACE2 complex without or with heparin bound (with heparin used as a model for HS), we demonstrate the ability of the polysaccharide chains and N-glycans to synergistically concur in dynamically and energetically

stabilizing the open spike:ACE2 complex. The heparin chains modulate the conformational dynamics of ACE2 and the spike NTD, promoting better packing of the complex. The simulations reveal that spike N17, N165 and N343 glycans and ACE2 N322 and N546 glycans act as a stabilizing buffer at the spike NTD:ACE2 interface. Consistently, previous reports showed that de-glycosylation of the spike N343 glycan drastically reduces spike RBD binding to ACE2 (Zheng et al., 2021), and that ACE2 N322 glycan interacts with spike glycoprotein (Capraz et al., 2021; Mehdipour & Hummer, 2021; Zhao et al., 2020).

Next, by performing enhanced sampling RAMD simulations, we demonstrate that heparin binding extends the residence time of the open spike-ACE2 complex, in agreement with (Cecon et al., 2022). In addition to the handshake role of the ACE2 N90 glycan described by others (Barros et al., 2021; Capraz et al., 2021; Kearns et al., 2022; Mehdipour & Hummer, 2021; Zhao et al., 2020), we find that stronger interactions between the spike and the ACE2 N90 glycan upon heparin binding and direct interaction between heparin and the ACE2 N53 glycan slow the dissociation of the complex, supporting the hypothesis that HS and the N-glycans may together contribute to strengthening the spike:ACE2 interaction.

Finally, by performing FDA analysis, we identified salt-bridge networks that, upon individual or combined substitution could yield prefusion-stabilized spikes that are more potent for inducing antibodies that neutralize SARS-CoV-2, as previously proposed for other mutations (Hsieh et al., 2020; Lu et al., 2022). Furthermore, we found that an intricate allosteric communication pathway triggered by ACE2 modulates the exposition of R815 and TMPRSS2-dependent viral entry, in agreement with previous reports (Low et al., 2022; Meng et al., 2022; Qing et al., 2022; Yu et al., 2022). Notably, we show that heparin/HS concur with ACE2 in modulating this allosteric communication pathway without shielding the previously identified binding site for antibodies targeting the fusion peptide (Low et al., 2022).

Based on the structural similarity between heparin and HS, we infer that HS and N-glycans exert a synergistic stabilizing effect on the spike:ACE2 complex, enhancing the SARS-CoV-2 infection by multiple mechanisms (see Fig. S19): (1) HS interacts with spike, facilitating the encounter of the virions with ACE2; (2) once spike is in the proximity of the human host cell receptor, the ACE2 N90 and N53 glycans have a pivotal role in spike:HS engagement and interaction, thereby stabilizing the protein:protein complex; (3) subsequently, HS guides the motion of ACE2 toward the NTD of the spike subunit to which ACE2 is bound, while the N-glycans of spike and ACE2 fill the space between the proteins, favoring a more densely packed S1:ACE2 complex and prolonging the residence time of the ACE2-spike complex; (4) ACE2 and HS binding prime the virus infection by promoting the exposition of the fusion peptide residues and the consequent cleavage of spike by TMPRSS2, thus destabilizing the packing and facilitating the subsequent release of the S1:ACE2 complex.

Since only the most abundant pattern of glycosylation for spike and ACE2, as well as one sulfation pattern for heparin/HS, was investigated, further simulations would be necessary to study the effects of variability in the N-glycan and heparin/HS sulfation pattern. Nevertheless, the current computational findings are broadly supported by experimental data reported in the literature, suggesting that the simulated systems represent a reliable model to study the mechanisms involving N-glycans and heparin/HS. In light of our results, the low rate of mutations in the glycosylation sites of SARS-CoV-2 spike variants of concern (VoCs) (Newby et al., 2023), along with their higher affinity to HS (Kim et al., 2023) than the Wuhan variant, suggest a potential compensatory mechanism exerted by HS and spike N-glycans to offset the elevated mobility of the VoCs RBms. This mechanism facilitates the encounter and interaction with ACE2 and, coupled with a strengthened interplay between HS, spike and

ACE2 N-glycans, results in a more stable complex with longer residence time, explaining the enhanced infectivity of the virus. To confirm this hypothesis and elucidate potential susceptibility mechanisms, quantitative assays of the interaction of SARS-CoV-2 spike VoCs with cells expressing HS and ACE2 mutated at N53 or N90 would be of interest.

In conclusion, from our models and simulations, we have identified modulatory effects of N-glycans and heparin/HS on the spike:ACE2 interaction and obtained new insights into the mechanism of SARS-CoV-2 viral infection. These results support the potential of heparin/HS mimetics as therapeutics and provide a structural and dynamic framework for developing novel mimetics with enhanced specificity for competing with HS for the binding of spike.

**STAR METHODS**

Detailed methods are provided in the online version of this paper and include the following:

- MODELING OF THE SYSTEMS
- CONVENTIONAL MD SIMULATION
- RAMD SIMULATION
- ANALYSIS OF MD SIMULATIONS
    - Root mean square deviation (RMSD)
    - Root mean square fluctuation (RMSF)
    - Hydrogen bond (H-bond) analysis
    - Residue contact probability
    - Dynamic cross-correlation matrix
    - Distance and angle calculations
    - Essential dynamics (ED)
    - Force distribution analysis (FDA)
    - Molecular mechanics-generalized Born surface area (MM/GBSA) energies

***Supplementary information***

This article contains supplementary information.

***Acknowledgments***

Stefan Richter, Camilo Aponte and Bernd Doser from Heidelberg Institute for Theoretical Studies are gratefully acknowledged for technical support. G. P., M.F., and R. C. W. thank the Klaus Tschira Foundation for support. G. P. and R. C. W. thank the Deutsche Forschungsgemeinschaft (DFG, German Research Foundation—Project number: 458623378 to R. C. W.) for financial support. G. P. was supported by the Artificial Intelligence Health Innovation Cluster (post-doc fellowship – 1st cohort) and by the Joachim Herz Stiftung (Add-on fellowship for Interdisciplinary Life Science – 8th cohort). G.P. was supported by the Innogly – Cost Action CA18103 network. M. F. was supported by Erasmus+, the CAPES/DAAD bi-nationally supervised doctoral degree (DAAD, Deutscher Akademischer Austauschdienst or German academic exchange service; CAPES, Coordenação de Aperfeiçoamento de Pessoal de Nível Superior or Coordination for the Improvement of Higher Education Personnel –Research grant number: 57507871). This publication was supported through state funds approved by the State Parliament of Baden-Württemberg for the Innovation Campus Health + Life Science Alliance Heidelberg Mannheim.

***Author contributions***

G. P., M. R., and R. C. W. conceptualization; G. P. and M.F. formal analysis; G. P., M.F. and R. C. W. funding acquisition; G. P. and M. F. investigation; G. P. methodology; R. C. W. resources; R. C. W. supervision; G. P. validation; G. P. visualization; G. P. writing—original draft; R. C. W. writing—review and editing.

***Declaration of interests***

The authors declare no competing interests.

## *Figure titles and legends*

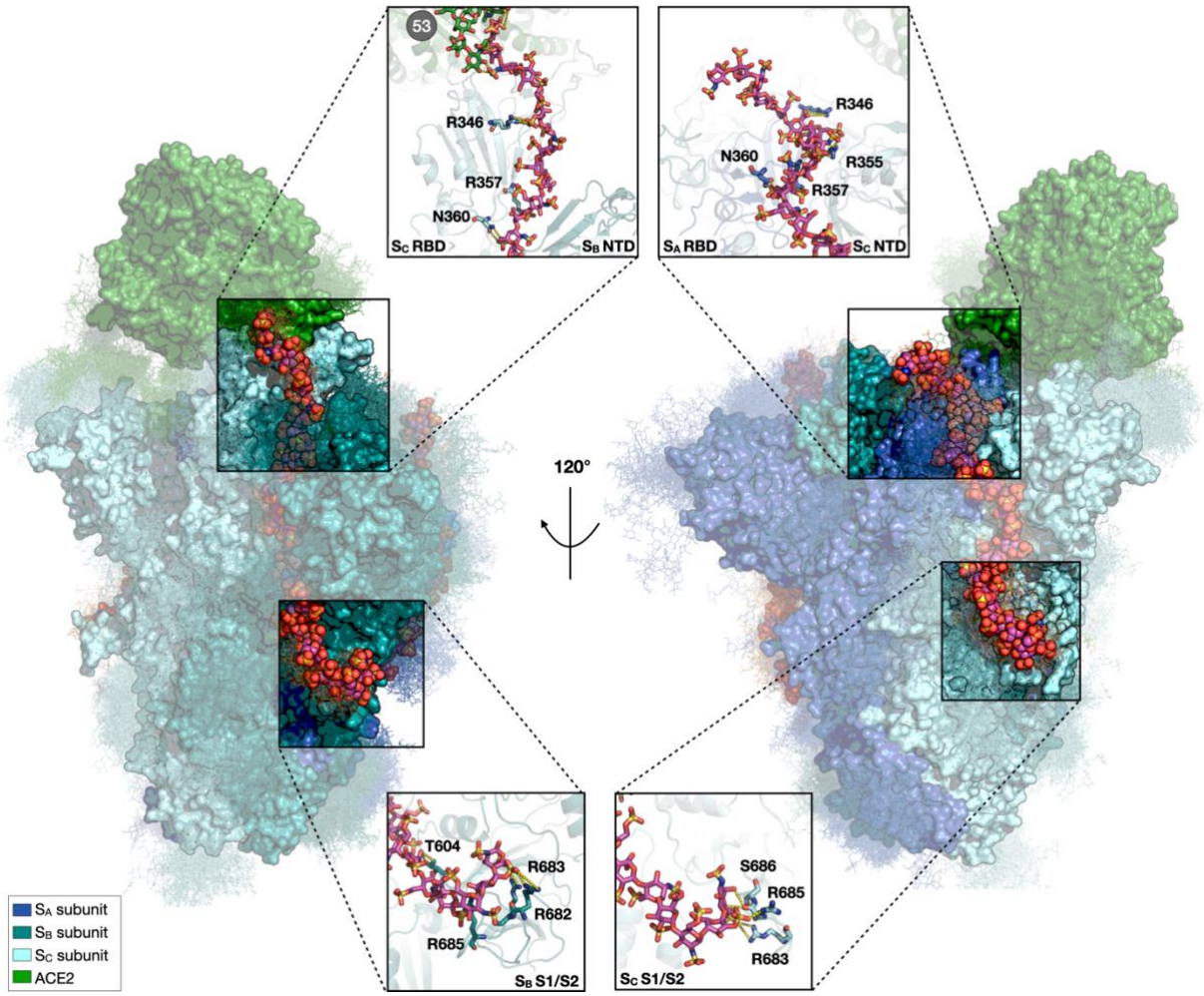


***Fig. 1 Structural model of the complex of the open, active spike homotrimer, the ACE2 RBD and three heparin chains, showing stabilizing interactions of two heparin chains and N-glycans with spike and ACE2.*** *Two side views of a representative structure obtained from the last snapshot of one of the MD simulation replicas are shown. $S_A$, $S_B$, and $S_C$ subunits and ACE2 are shown as molecular surfaces in blue, teal, cyan, and green, respectively. N-glycans covalently attached to the spike and ACE2 are shown in line representation, colored according to the subunit to which they are attached. 40 frames of the N-glycan structures collected at intervals of 25 ns from the simulation are shown. The 31mer heparin chains are depicted as spheres colored by element with magenta carbons. On the left, heparin2 spans from the $S_C$ up-RBD to the $S_B$ S1/S2 multifunctional domain. On the right, heparin3 follows a similar path, simultaneously binding the $S_A$ down-RBD and the $S_C$ NTD and S1/S2.*

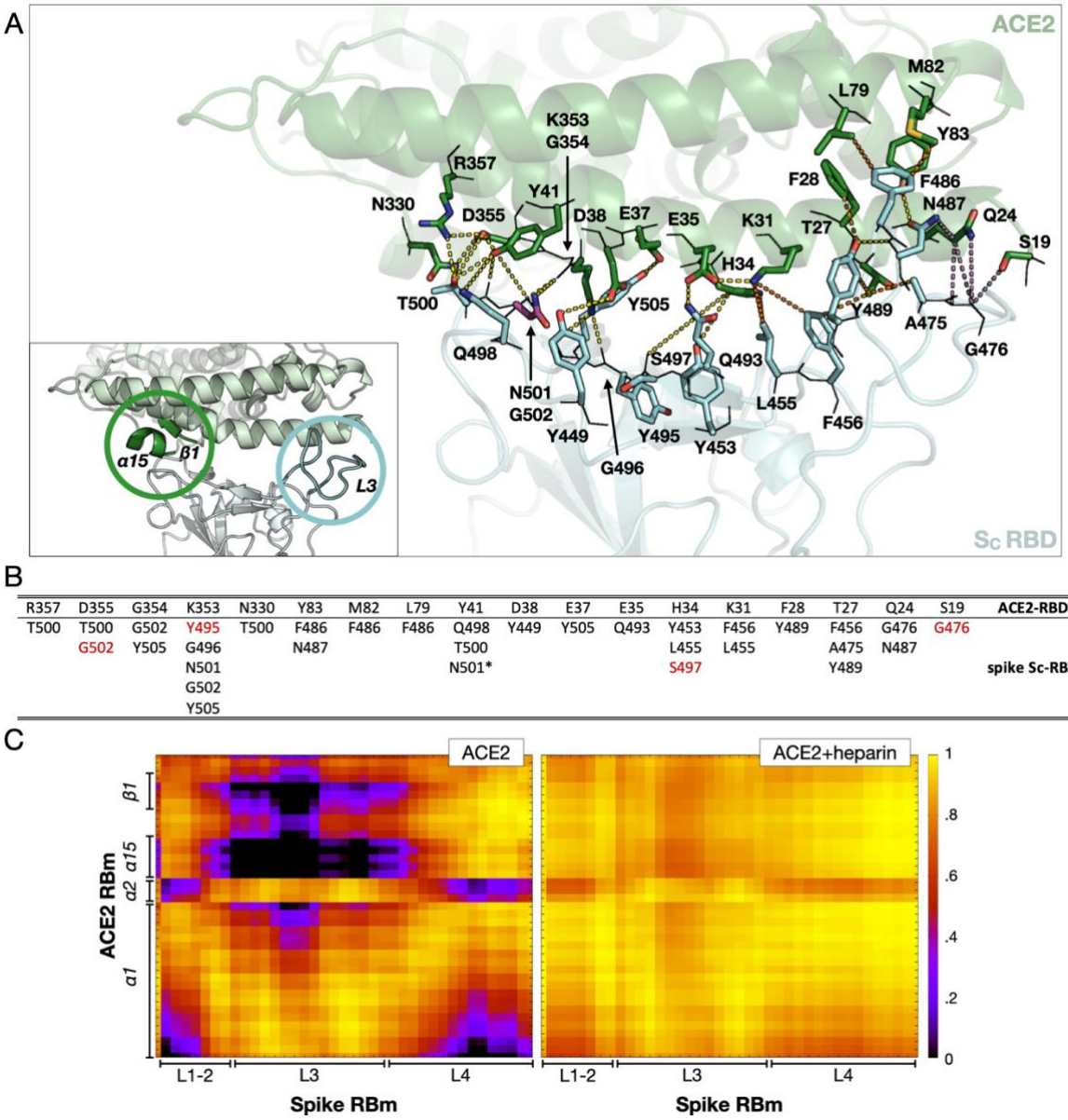


***Fig.2 Binding of heparin alters the interactions at the interface between the spike $S_C$ subunit (up-RBD) and ACE2. (A)*** *View of the $S_C$ RBD – ACE2 interface extracted from the last snapshot of the replica 1 trajectory simulated in the presence of heparin. The $S_C$ RBD and ACE2 are shown as cartoons colored cyan and green, respectively. Heparin is not shown for clarity. Residues involved in the interactions are labeled and depicted as lines (main chains) and sticks (side chains) colored by element with oxygen, nitrogen, and sulfur in red, blue, and yellow, respectively. N501 is shown as magenta stick colored by element. Dashes connect interacting residues are colored yellow, orange, and violet to differentiate between polar, hydrophobic, and other types of contact, respectively. The contact residue pairs (cutoff = 3.5 Å) with occupancies higher than 90% are labelled. Contact matrices for each replica are given in Fig. S4. The inset shows the location in the 3D structure of two regions of spike $S_C$ RBD and ACE2 that are dynamically coupled in the presence of heparin (see C). (B) Interactions between ACE2 (upper line) and $S_C$ RBD. Residues colored red gained the respective interactions during the simulations (both with and without heparin) compared to the interactions reported in the literature (Lan et al., 2020; Shang et al., 2020)*; see *Tab. S1. The asterisk for the Y41-N501 interaction indicates that it is lost only in simulations with heparin chains. (C) Dynamic cross-correlation matrices of residues of $S_C$ RBm (x-axis) and ACE2-RBm (y-axis) for the spike:ACE2 (left) and spike:ACE2:heparin (right) systems. Values range from 0 (black, uncorrelated motion) to +1 (yellow, correlated motion). The plots are shown for the replica 1 trajectory; plots for all replica trajectories are available in Fig. S5. Fig. S6 shows the secondary structure prediction and the position in the 3D structure of the regions considered for the analysis.*

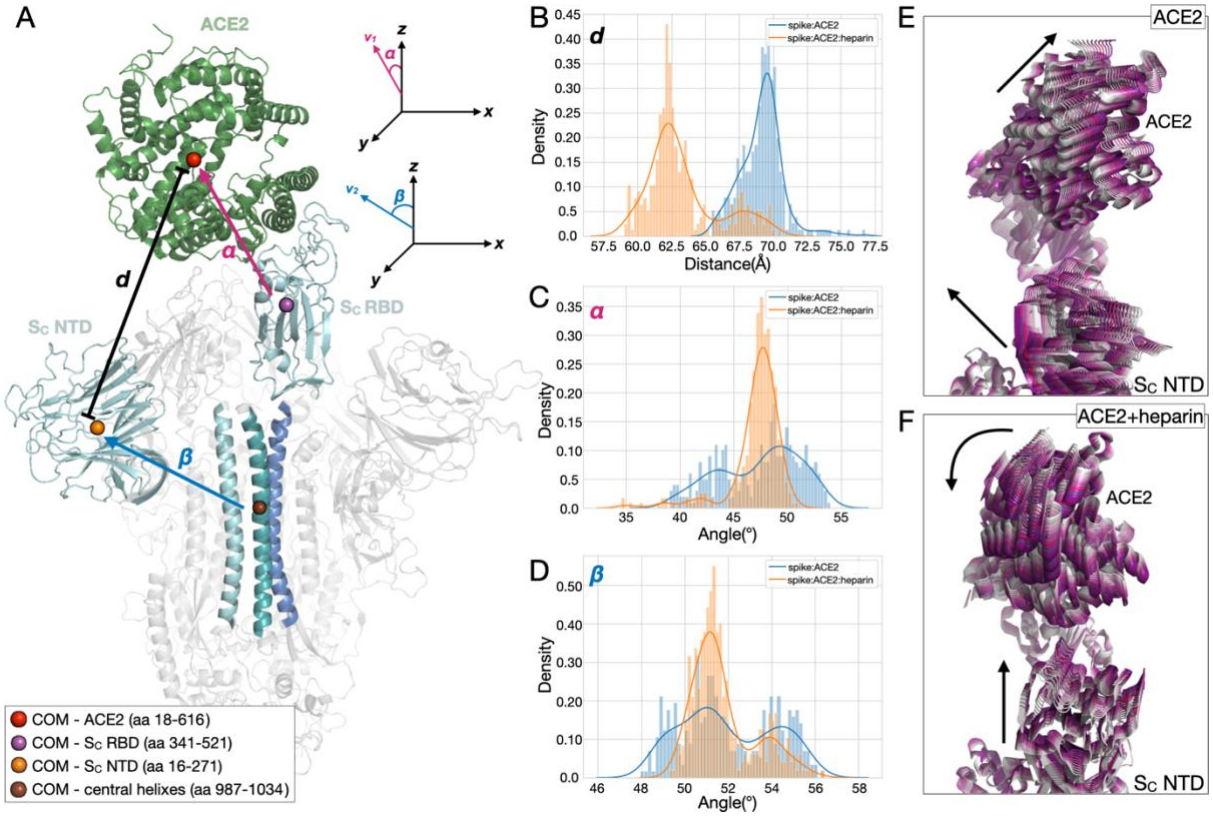


***Fig. 3 ACE2 and the $S_C$ NTD approach each other in the presence of heparin.*** *(A) Side view of a representative structure of the spike head ectodomain in the open conformation ($S_C$ with up-RBD) in complex with ACE2. Spike and ACE2 are shown as cartoons colored grey and green, respectively. The $S_C$ RBD, NTD, and central helix are colored cyan. The $S_A$ and $S_B$ central helices are colored marine and teal, respectively. The spheres represent the center of mass (COM) calculated for each domain and are colored red, violet, orange and brown for ACE2 (residues 18-616), $S_C$ RBD (residues 341-521), $S_C$ NTD (residues 16-271), and the three spike central helices (residues 987-1034), respectively. To define the approach of ACE2 and the spike, the complex was oriented perpendicular to the xy plane. The distance **d** and vectors **v1** and **v2** were defined as follows: **d** (black) is the distance between the COM of ACE2 and the COM of $S_C$ NTD; **v1** (magenta) points from the COM of the $S_C$ RBD to the COM of ACE2; **v2** (blue) points from the COM of the three central helices to the COM of the $S_C$ NTD. The relative position of ACE2 is defined by (B) the distance **d**, and the angles α (C) and β (D) between the z-axis and **v1** and **v2,** respectively. The distributions (B-D) were calculated from the MD trajectories for all replicas and are colored according to system: spike:ACE2 (blue) and spike:ACE2-heparin (orange). The distance between the COMs is reduced upon heparin binding and the α and β angles adopt narrower distributions. The motion of ACE2 and the $S_C$ RBD in the absence (E) and presence (F) of heparin is shown by the superimposition of ten conformations extracted at equal time intervals along a representative trajectory (from grey to purple) and projected onto the first essential dynamics eigenvector. ACE2 and $S_C$ RBD are shown in cartoon representation, with heparin omitted for ease of visualization. The corresponding plots for all the replica trajectories are similar and are shown in Fig. S8.*

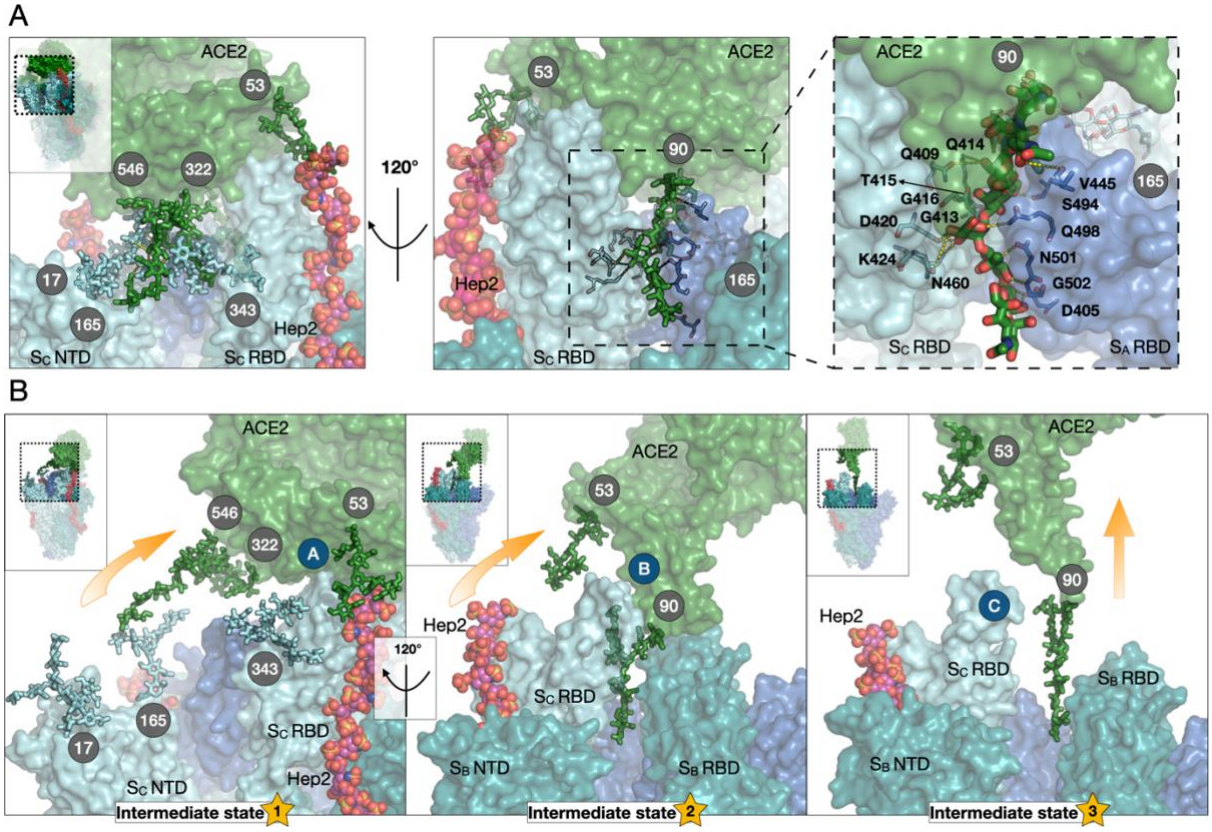


***Fig. 4 N-glycans and heparin contribute to stabilization of the open spike:ACE2 complex and hinder its dissociation.*** *(A) Interactions established by the N-glycans in the conventional MD simulations: buffering effect of spike and ACE2 N-glycans at the interface between ACE2 and $S_C$ NTD (left); ACE2 N53 glycan-heparin interactions and insertion of ACE2 N90 glycan at the interface between $S_C$ RBD and $S_A$ RBD (center) with an enlargement showing the interactions established by the N90 glycan with the spike residues (right). (B) The dissociation pathway of ACE2 from spike in the presence of heparin observed in the RAMD trajectories has three intermediate states. Yellow arrows show the dissociation route of ACE2 as a fan-like rotational movement in the first two intermediate states and a translating movement in the third. Blue circles (labelled A-C) highlight changes in the protein:protein interactions along the dissociation pathway schematically. $S_A$, $S_B$, and $S_C$ subunits and ACE2 are shown as surfaces in blue, teal, cyan, and green, respectively. Mechanistically key N-glycans covalently attached to spike and ACE2 are labeled with grey circles and shown in stick representation, colored according to the subunit to which they are attached. The 31mer heparin chain bound to the $S_C$ up-RBD is depicted as spheres colored by elements with magenta carbons. For further details of the dissociation pathway, see Figs. S11-S13.*

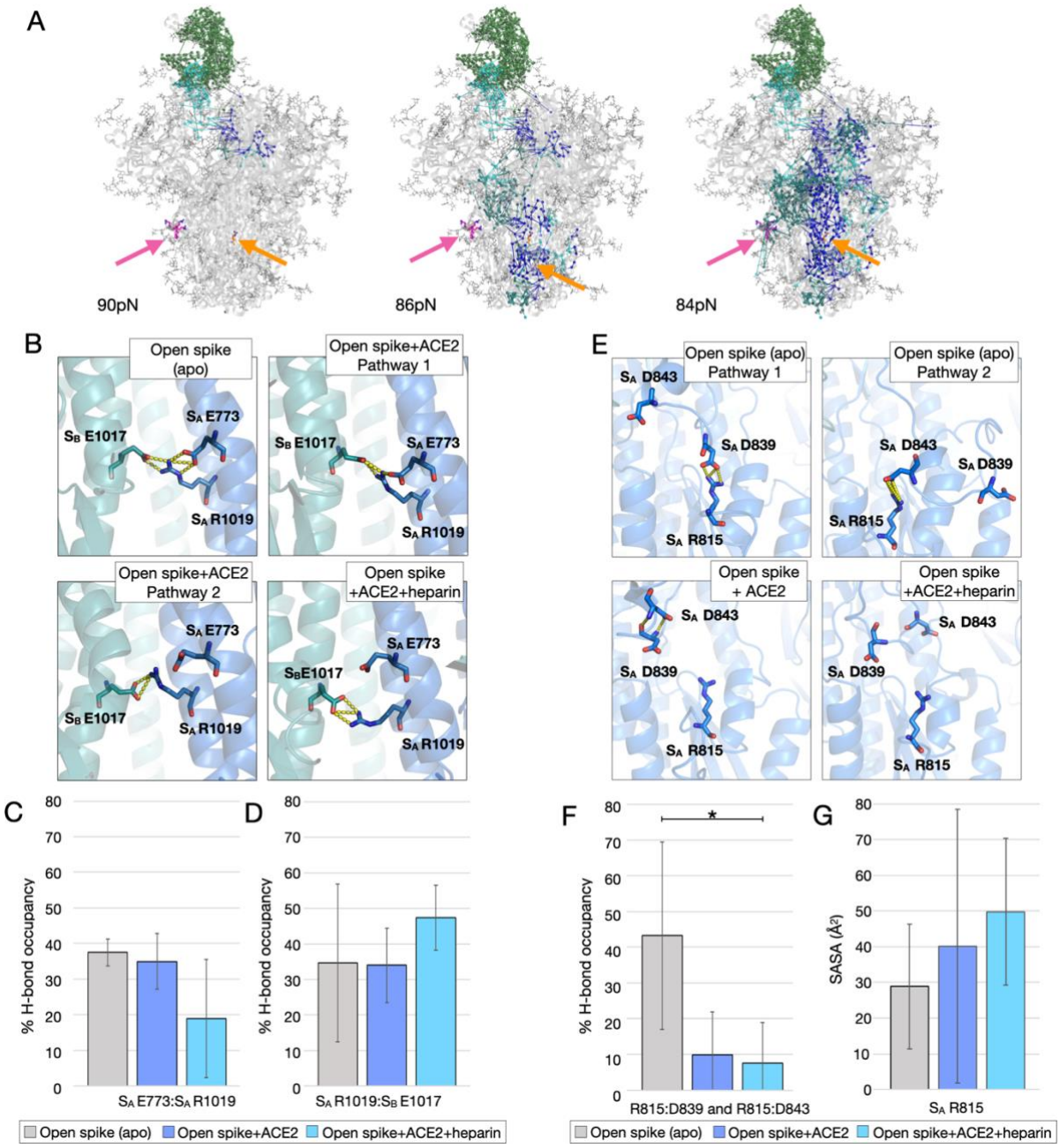


***Fig. 5 The binding of ACE2 and heparin allosterically affects the spike protease cleavage sites, promoting virus priming.*** *(A) Residue-based pairwise force differences in the open spike protein when bound to ACE2 compared to when not bound to ACE2 at three force thresholds (lines). The residue-based pairwise force difference upon heparin binding (not shown for clarity) follows the same distribution pattern. The spike and ACE2 glycoproteins are shown as grey cartoons with lines representing the N-glycans. Pairwise force vectors are depicted as lines colored according to the location of the initial point residue (marine, teal, cyan, and green for $S_A$, $S_B$, $S_C$, and ACE2, respectively). The key residues, R815 and the S1/S2 functional site residues, are shown in orange and magenta, respectively. (B) Proposed force transduction from $S_A$ E773 to $S_A$ R1019 and $S_A$ E1017 (in the central helices – yellow dashed lines represent H-bonds) and (C-D) the relative trajectory-averaged H-bond occupancy calculated for the last 400ns of the MD simulations. (E) Proposed force transduction from $S_A$ R815 (cleavage site of TMPRSS2) to $S_A$ D839 and $S_A$ D843 (in the fusion peptide - yellow dashed lines represent the H-bonds) and (F) the relative trajectory-averaged H-bond occupancy calculated for the last 400ns of the MD simulations. The solvent-accessible surface area (SASA) of $S_A$ R815 along the corresponding trajectories is reported in (G) and shows that binding of ACE2 alone or ACE2 and heparin tends to increase the exposure of the residue. Data are presented as mean ± SEM. *$p < 0.05$, two-tail ANOVA.*

## *Tables with titles and legends*

| | ***Heparin1 (down-RBD)*** | ***Heparin2 (up-RBD)*** | ***Heparin3 (down-RBD)*** |
|---|---|---|---|
| *Spike RBD* | $S_B$: T345, R346, R357, S359, N360 | $S_C$: R346, R357, N360 | $S_A$: R346, R355, R357, N360 |
| *Spike NTD* | $S_A$: T167, T208 | $S_B$: Q173, L176, T286, D287 | $S_C$: N280, N282, T284 |
| *Spike S1/S2* | $S_A$: R682, R683, R685, S689 | $S_B$: T604, R682, R683, R685 | $S_C$: R683, R685, S686 |
| *Spike N-glycans* | $S_A$: N122, N149, N165, N282<br>$S_B$: N331 | $S_B$: N109, N149, N296<br>$S_C$: N331 | $S_C$: N122, N282<br>$S_A$: N331 |
| *ACE2 N-glycans* | - | ACE2: N53 | - |

***Tab. 1 Residues in functional sites in open spike and N-glycans in spike and ACE2 make H-bonds with the heparin chains.*** H-bond interactions were computed over the 6 replica simulations in the presence of heparin and are given for each spike functional site (RBD, NTD, S1/S2, N-glycans) of each subunit ($S_A$, $S_B$ or $S_C$) as well as for ACE2 N-glycans. No direct H-bond interactions were observed between the heparin chains and ACE2 amino-acid residues. Residues are shown in the 3D structure in Fig. 1, and H-bond occupancies are given in Fig. S2.

| *N-glycans* | *System* | $\Delta G^{total}$ | $\Delta G^{el}$ | $\Delta G^{VdW}$ | $\Delta G^{solv}$ |
|---|---|---|---|---|---|
| + | *Spike:ACE2* | -105.88 ± 5.79 | -2777.50 ± 109.17 | -305.19 ± 37.06 | 2976.81 ± 137.04 |
| | *Spike:ACE2+heparin* | -123.20 ± 37±.03 | 17725.09 ± 693.54 | -352.81 ± 73.55 | -17541.18 ± 733.45 |
| + | *$S_C$ RBD:ACE2* | -69.96 ± 6.12 | -881.69 ± 37.71 | -171.41 ± 7.74 | 971.64 ± 47.65 |
| | *$S_C$ RBD:ACE2+heparin* | -49.18 ± 13.13 | 6302.11 ± 358.87 | -147.61 ± 15.12 | -6205.29 ± 404.03 |
| - | *$S_C$ RBD+NTD:ACE2* | -33.21 ± 12.94 | -1232.56 ± 80.39 | -116.08 ± 21.45 | 1315.43 ± 99.09 |
| | *$S_C$ RBD+NTD:ACE2+heparin* | -43.76 ± 16.08 | 5564.62 ± 431.00 | -140.07 ± 24.37 | -5471.27 ± 443.07 |
| + | *$S_C$ RBD+NTD:ACE2* | -72.17 ± 12.94 | -1457.42 ± 111.47 | -236.48 ± 46.85 | 1621.74 ± 138.99 |
| | *$S_C$ RBD+NTD:ACE2+heparin* | -86.04 ± 35.94 | 5649.30 ± 435.47 | -260.60 ± 57.99 | -5477.17 ± 460.36 |

***Tab. 2 Computed binding free energies indicate that the heparin chains and N-glycans energetically stabilize open spike:ACE2 complexes****. Their effect is exerted primarily through favorable van der Waals packing interactions**.** Computed MM/GBSA energies (kcal/mol) and their energy components are given for the spike:ACE2, $S_C$ RBD:ACE2, and $S_C$ RBD+NTD:ACE2 interactions in the absence and in the presence of heparin. – or + denotes that glycans are excluded or included in the computation. The averages and standard deviations of the energy values are computed from the replica simulations of the spike:ACE2 (4 trajectories) and spike:ACE2:heparin (6 trajectories) systems.*

## STAR METHODS

**Modeling of the systems**. The two starting structures of the ectodomain of the spike glycoprotein of the Wuhan variant (UniProt A0A679G9E9) in an open, active conformation either with or without three heparin chains bound were the initial structures built by Paiardi et al (Paiardi et al., 2022). The three heparin chains (hereafter referred to as heparin1, heparin2 and heparin3) were previously modelled using the sliding window method developed by Bugatti and co-workers (Bugatti et al., 2019) and span from the RBD of one spike subunit (the $S_B$, $S_C$ or $S_A$ subunit) to the NTD and S1/S2 functional domains of the adjacent spike subunit (the $S_A$, $S_B$ or $S_C$ subunit, respectively). The coordinates for the complex of the ACE2 RBD (hereafter referred to as ACE2) with the spike RBD were retrieved from the RCSB: PDBid 6M0J (Lan et al., 2020) and superimposed on the spike RBD of the starting structures. The spike RBD from the ACE2-spike complex was then removed while retaining

the $Zn^{2+}$ ion. The ACE2 was fully glycosylated by adding 6 N-glycans by following the available glycomic profile (Zhao et al., 2020) and using the Glycam website (http://glycam.org/). The protonation state was computed at neutral pH using PROPKA (Li et al., 2005) and PDB2PQR (Dolinsky et al., 2004). None of the spike or ACE2 titratable residues show an unusual protonation state. The two models of the spike:ACE2 and spike:ACE2:heparin complexes were then solvated and equilibrated for all-atom Molecular Dynamics (MD) simulation.

**Conventional MD simulation**. All conventional MD simulations were carried out using the Amber 20 software (Case & Belfon, 2020). The Amber ff14SB (Maier et al., 2015), GLYCAM-06j (Kirschner et al., 2008) and general AMBER (GAFF) (Wang et al., 2004) force fields were used to assign the parameters. The starting configurations were solvated in the center of a cubic periodic solvent box using a TIP3P water model (Pekka & Lennart, 2001) with at least 10 Å between the solutes and the edges of the box. Na+ and Cl- ions were added to neutralize the systems and to immerse them in solvent with an ionic strength of 150 mM. The two final models of the spike:ACE2 and spike:ACE2:heparin consist of 873223 and 872404 atoms, respectively. Energy minimization was performed in 14 consecutive energy minimization steps, each of 100 steps of steepest descent followed by 900 steps of conjugate gradient, with decreasing positional restraints from 1000 to 0 kcal/mol $A^2$ on all the atoms of the systems excluding waters, counterions, and hydrogens, with a cutoff for Coulombic and Lennard-Jones nonbonded interactions of 8 Å. Subsequently, the systems were subjected to two consecutive steps of heating, each of 100,000 time steps, from 10 to 100 K and from 100 to 310 K in an NVT ensemble with a Langevin thermostat. Bonds involving hydrogen atoms were constrained with the SHAKE algorithm[32], and 2 fs time step was used. The systems were then equilibrated at 310 K in four consecutive steps of 2.5 ns each in the NPT ensemble with a Langevin thermostat and a Berendsen barostat with random velocities assigned at the beginning of each step. Then multiple independent 1µs MD production runs for the systems without (4x) and with heparin (6x) were carried out starting from randomly chosen restart files with randomly assigned velocities from the last 5 ns of equilibration. Short-ranged nonbonded interactions (Coulombic and Lennard-Jones) were evaluated using a cutoff of 8 Å, while long-range electrostatic interactions were treated using the Particle Mesh Ewald method (Essmann et al., 1995). Temperature was maintained at 310 K using the Langevin thermostat while pressure was controlled using the Berendsen barostat with a 0.4 ps relaxation time. Coordinates were written at intervals of 100 ps. Simulations were carried out on in-house GPU-nodes.

**RAMD simulations.** The last snapshot of each conventional MD replica simulation was used as the starting point for the random acceleration molecular dynamics (RAMD) simulations (Kokh et al., 2018; Kokh et al., 2020). For each of these snapshots, the Amber format files (coordinates and topology) were converted to GROMACS format using the AnteChamber Python Parser interfacE (acpype) script (Sousa Da Silva & Vranken, 2012). The periodic box was enlarged by 70 Å along the z-axis to allow the glycoproteins to separate during the simulations and refilled with TIP3P water molecules and ions to maintain 150 mM NaCl concentration, reaching 900170 and 1061017 atoms for spike:ACE2 and spike:ACE2:heparin systems, respectively. Each system was geometry-optimized using up to 50,000 steepest descent steps until the maximum force was lower than 100 $kJ.mol^{-1}nm^{-1}$. The system was then heated in the NVT ensemble for 100 ps to a target temperature of 310 K using a time step of 1 fs, a Langevin thermostat with a friction coefficient of 0.5 $ps^{-1}$, and position restraints of 1000 $kJmol^{-1}nm^{-2}$ on the solute atoms. The system was then equilibrated with no restraints for 1 ns in the NPT ensemble using the Langevin thermostat with a friction

coefficient of 0.5 $ps^{-1}$ and the Berendsen barostat with a 0.4 ps relaxation time. The equilibration was extended for a further 2.5 ns using a 2 fs time step. For all equilibration simulations, the GROMACS 2020.3 (Van Der Spoel et al., 2005) engine was used. After equilibration, 15 dissociation trajectories were generated for each replica using the RAMD method implemented in GROMACS-RAMD (https://github.com/HITS-MCM/gromacs-ramd). During the equilibration and dissociation simulation, short-ranged nonbonded interactions (Coulombic and Lennard-Jones) were treated using a 12 Å cut-off, and electrostatic interactions were treated with the fast smooth Particle-Mesh Ewald scheme (Essmann et al., 1995). An additional force with random initial orientation and 120 kcal/mol Å magnitude was applied to the center of mass (COM) of ACE2. The movement of ACE2 was monitored at intervals of 50 time steps and, if ACE2 did not move more than 0.025 Å in one of these intervals, the direction of the force was changed randomly and the simulation continued. The simulations were stopped when the proteins had dissociated such that the distance between the COMs of spike and ACE2 exceeded 120 Å. For the RAMD simulations, the leap-frog integrator was used with a 2 fs timestep. The pressure (1 atm) and temperature (310 K) were kept constant using the Parrinello-Rahman barostat (Parrinello et al., 1981) and Nóse-Hoover thermostat (Evans & Holian, 1985), respectively.

**Analysis of MD simulations**. VMD (Humphrey et al., 1996) was employed for visual inspection of the trajectories, and used along with CPPTRAJ (Roe & Cheatham, 2013) from AmberTools20 (Case & Belfon, 2020) for quantitative analysis.

*Root mean square deviation (RMSD) and Root mean square fluctuation (RMSF)* were computed using CPPTRAJ (Roe & Cheatham, 2013) for all C-alpha atoms of the spike subunits - $S_A$, $S_B$, $S_C$ - as well as for ACE2 and for all the carbon, oxygen, sulfur and nitrogen atoms of each heparin chain (heparin1, heparin2, heparin3) (Fig. S1). The RMSF of the spike $S_C$ RBD with and without heparin chains bound was calculated for the C-alpha atoms of residues 341-521 (Fig. S7).

*Hydrogen bond (H-bond) analysis* was performed with VMD (Humphrey et al., 1996) using a single trajectory approach and subsequently computing the statistics (average and standard deviations) over the replica simulations of each system (Fig. 2A,5B-C and S2-3, S9, S12, S17). H-bonds were computed using the default parameters (donor hydrogen-acceptor distance of less than 3Å and D-H…A angle cut off maximum of 20°) for the converged parts of the trajectories (400 ns to 1 microsec) or for the last 400ns in association with FDA analyses or on the last 100 ps of the RAMD trajectories and are reported only when present in at least 50% of the replicas (i.e. in at least 2 and 3 replicas for systems without and with heparin, respectively). Occupancy was determined by counting the number of frames in which a specific hydrogen bond was formed with respect to the total number of frames.

*- H-bonds of heparin* were computed between each heparin chain and the spike and ACE2 glycoproteins (Fig. S2, S12). Given the hydrophilic nature of heparin, H-bonds are expected to represent the major interactions established with the amino acid residues. Therefore, no further interactions were computed. H-bonds were computed using the default parameters and a cut-off occupancy level of 10% was used.

*- H-bonds between protein residues* were computed for amino acid residues 417-505 and 19-393 of spike $S_C$ RBD and ACE2 RBD, respectively, using a cut-off occupancy of 10% (Fig. 2A, S3A, S12B), while the number of contacts during the trajectories for Fig. S3A is reported in Fig. S3B.

- *H bonds of N*-glycans were computed for spike $S_C$ N17, N165, N322, N657 glycans with ACE2 glycoprotein and for ACE2 N90, N322 and N546 glycans with spike glycoprotein (Fig. S9, S12C) and for $S_B$ N657 with the $S_C$ D439 residue (Fig. S17). Given the polar nature of the monosaccharides, H-bonds are expected to represent the major interactions with the amino acid residues. No further interactions were computed. H-bonds were considered using a cut-off occupancy level of 10%.

*Residue contact probability* (percentage of total simulation time during which residues are in contact) was computed with an in-house *tcl* script for VMD (Humphrey et al., 1996) between amino acid residues 417-505 and 19-393 of spike $S_C$ RBD and ACE2 RBD, respectively, using a single trajectory approach and subsequently computing the statistics (average and standard deviations) over the replica simulations of each system (Fig. 2A-B and S4, S12A). Contacts were computed considering a maximum residue-residue contact distance of 3.5 Å for the converged parts of the conventional MD trajectories (from 400ns to 1 microsec) and for the last 100ps of the RAMD trajectories and are plotted in the matrix when identified in at least 1 frame of a trajectory and present in at least 50% of the replicas (i.e. in at least 2 or 3 replicas for systems without or with heparin, respectively).

*Dynamic cross-correlation matrices* were computed using CPPTRAJ (Roe & Cheatham, 2013) and were based on per-residue Pearson's correlation coefficients (CCs) as derived from the mass-weighted covariance matrices calculated for residues at the interface between the ACE2 RBm and the spike $S_C$ RBm (Fig. 2C and S5).

*Distance and angle calculations* were performed using an in-house *tcl* script with VMD (Humphrey et al., 1996) (Fig.3). To define the orientation of the protein, the complex was aligned with the reference structure, perpendicular to the xy-axis. The distance between ACE2 and the spike $S_C$ NTD was computed between the COMs of ACE2 (residues 18-616) and the $S_C$ NTD (residues 16-271). The alpha and beta angles were computed between the z-axis and the vectors $\boldsymbol{v_1}$ and $\boldsymbol{v_2}$. Vector $\boldsymbol{v_1}$ spans from the COM of the up-RBD of the $S_C$ subunit (residues 341-521) to the COM of ACE2, whereas vector $\boldsymbol{v_2}$ spans from the COM of the three spike central helices (residues 987-1034) to the COM of the $S_C$ NTD. Distances and angles were computed at each frame along the trajectories as a deviation (positive or negative) from their initial values. The trajectories were aligned to the reference structure at frame 0 of each independent trajectory.

*Essential dynamics (ED)* analysis consisted of Principal Component Analysis (PCA) of the conventional MD simulations. PCA was performed along the individual trajectories with CPPTRAJ (Roe & Cheatham, 2013). The principal modes of motion were visualized using VMD (Humphrey et al., 1996).The first normalized eigenvectors for the subsystem of spike $S_C$ and ACE2 without and with heparin bound were plotted along the trajectory, and the direction of motion was defined by visual inspection (Figs. 3E-F and S8).

Force distribution analysis (FDA) implemented in a modified version of GROMACS 2020.4 (Van Der Spoel et al., 2005) available at (https://github.com/HITS-MBM/gromacs-fda) was used to calculate the changes in internal forces in the spike and ACE2 glycoproteins upon binding of heparin (Fig. 5 and S14-S16). For details on the methodology, see (Costescu & Gräter, 2013). To perform FDA, the Amber format files (coordinates, topology, trajectory files) were first stripped of water and ions and then converted to GROMACS format using the AnteChamber Python Parser interfacE (acpype) script (Sousa Da Silva & Vranken, 2012). FDA was performed on each individual trajectory per condition and the resulting average pairwise forces of the apo state were subtracted from those of the holo state. The networks shown are connected edges for at least 3 residues with force differences above a given threshold

(Fig. 5A). The punctual stress is the sum of the absolute values of scalar pairwise forces acting on each atom (Fig. S14-S16). Forces from water and ions were not considered in this analysis due to their rapid interchange of positions. However, the force distribution pattern indirectly reflects the effect of the solvent, as the MD simulations were carried out in explicit aqueous solution at physiological ion concentration.

*Molecular mechanics-generalized Born surface area (MM/GBSA) energies* were computed with AmberTools20 (Case & Belfon, 2020) (python script) using a single trajectory approach and then computing the average and standard deviation over the replica simulations of each system (Tab. 2). Binding affinities were calculated for systems without and with heparin using the last 5000 frames (corresponding to the last 500 ns) of each conventional MD trajectory. Water molecules and ions were treated implicitly (igb=2 and saltconc=0.15 M). All other parameters were assigned default values. MM/GBSA energies were computed for the following systems without and with heparin: (i) spike:ACE2 including N-glycans; (ii) spike $S_C$ RBD:ACE2 excluding glycans; (iii) spike $S_C$ NTD+RBD:ACE2 including N-glycans (iv) spike $S_C$ NTD+RBD:ACE2 excluding N-glycans. The $S_C$ RBD was defined by residues 341-521, whereas the $S_C$ NTD consisted of residues 16-271 (Tab. 2).

**DATA AND CODE AVAILABILITY**

Conventional MD simulation replica trajectories of spike:ACE2 complexes in the absence and the presence of heparin are available on the BioExcel COVID-19 platform https://bioexcel-cv19.bsc.es/#/ with the identifiers MCV1901746 and MCV190174, respectively. All data that support the findings of this study are publicly available in the Zenodo repository: https://zenodo.org/records/10617411. All software used is available as described in the Methods. BiorXiv preprint server XXX..

**REFERENCE**


Barros, E. P., Casalino, L., Gaieb, Z., Dommer, A. C., Wang, Y., Fallon, L., . . . Amaro, R. E. (2021). The flexibility of ACE2 in the context of SARS-CoV-2 infection. *Biophys J*, *120*(6), 1072-1084. https://doi.org/10.1016/j.bpj.2020.10.036

Bugatti, A., Paiardi, G., Urbinati, C., Chiodelli, P., Orro, A., Uggeri, M., . . . Rusnati, M. (2019). Heparin and heparan sulfate proteoglycans promote HIV-1 p17 matrix protein oligomerization: computational, biochemical and biological implications. *Scientific Reports*, *9*(1). https://doi.org/10.1038/s41598-019-52201-w

Capraz, T., Kienzl, N. F., Laurent, E., Perthold, J. W., Föderl-Höbenreich, E., Grünwald-Gruber, C., . . . Stadlmann, J. (2021). Structure-guided glyco-engineering of ACE2 for improved potency as soluble SARS-CoV-2 decoy receptor. *Elife*, *10*. https://doi.org/10.7554/eLife.73641

Casalino, L., Gaieb, Z., Goldsmith, J. A., Hjorth, C. K., Dommer, A. C., Harbison, A. M., . . . Amaro, R. E. (2020). Beyond Shielding: The Roles of Glycans in the SARS-CoV-2 Spike Protein. *ACS Central Science*, *6*(10), 1722-1734. https://doi.org/10.1021/acscentsci.0c01056

Case, D. A., & Belfon, K. B.-S., I.Y. Brozell, S.R. Cerutti, D.S. Cheatham, T.E. Cruzeiro, V.W.D. Darden, T.A. Duke, R.E. Giambasu, G. Gilson, M.K. Gohlke, H. Goetz, A.W. Harris, R.Izadi, S. Izmailov, S.A. Kasavajhala, K. Kovalenko, A. Krasny, R. Kurtzman, T. Lee, T.S. LeGrand, S.Li, P. Lin, C. Liu, J. Luchko, T. Luo, R. Man, V. Merz, K.M. Miao, Y. Mikhailovskii, O. Monard, G. Nguyen, H. Onufriev, A. Pan, F. Pantano, S. Qi, R. Roe,

D.R. Roitberg, A. Sagui, C. Schott-Verdugo, S. Shen, J. Simmerling, C.L. Skrynnikov, N.R. Smith, J. Swails, J. Walker, R.C. Wang, J. Wilson, L. Wolf, R.M. Wu, X. Xiong, Y. Xue, Y. York, D.M. Kollman, P.A. (2020). *AMBER 2020*. In University of California, San Francisco.

Cecon, E., Burridge, M., Cao, L., Carter, L., Ravichandran, R., Dam, J., & Jockers, R. (2022). SARS-COV-2 spike binding to ACE2 in living cells monitored by TR-FRET. *Cell Chemical Biology*, *29*(1), 74-83.e74. https://doi.org/10.1016/j.chembiol.2021.06.008

Clausen, T. M., Sandoval, D. R., Spliid, C. B., Pihl, J., Perrett, H. R., Painter, C. D., . . . Esko, J. D. (2020). SARS-CoV-2 Infection Depends on Cellular Heparan Sulfate and ACE2. *Cell*, *183*(4), 1043-1057.e1015. https://doi.org/10.1016/j.cell.2020.09.033

Costescu, B. I., & Gräter, F. (2013). Time-resolved force distribution analysis. *BMC Biophysics*, *6*(1), 5. https://doi.org/10.1186/2046-1682-6-5

Dodero-Rojas, E., Onuchic, J. N., & Whitford, P. C. (2021). Sterically confined rearrangements of SARS-CoV-2 Spike protein control cell invasion. *Elife*, *10*. https://doi.org/10.7554/eLife.70362

Dolinsky, T. J., Nielsen, J. E., McCammon, J. A., & Baker, N. A. (2004). PDB2PQR: an automated pipeline for the setup of Poisson-Boltzmann electrostatics calculations. *Nucleic Acids Res*, *32*(Web Server issue), W665-667. https://doi.org/10.1093/nar/gkh381

Essalmani, R., Jain, J., Susan-Resiga, D., Andréo, U., Evagelidis, A., Derbali, R. M., . . . Seidah, N. G. (2022). Distinctive Roles of Furin and TMPRSS2 in SARS-CoV-2 Infectivity. *J Virol*, *96*(8), e0012822. https://doi.org/10.1128/jvi.00128-22

Essmann, U., Perera, L., Berkowitz, M. L., Darden, Tom, Lee, H., . . . G., L. (1995). A smooth particle mesh Ewald method In (Vol. 103, pp. 8577–8593): The Journal of Chemical Physics.

Evans, D. J., & Holian, B. L. (1985). The Nose–Hoover thermostat. In (Vol. 83, pp. 4069–4074).

Grant, O. C., Montgomery, D., Ito, K., & Woods, R. J. (2020). Analysis of the SARS-CoV-2 spike protein glycan shield reveals implications for immune recognition. *Scientific Reports*, *10*(1). https://doi.org/10.1038/s41598-020-71748-7

Harbison, A. M., Fogarty, C. A., Phung, T. K., Satheesan, A., Schulz, B. L., & Fadda, E. (2022). Fine-tuning the spike: role of the nature and topology of the glycan shield in the structure and dynamics of the SARS-CoV-2 S. *Chemical Science*, *13*(2), 386-395. https://doi.org/10.1039/d1sc04832e

Hoffmann, M., Kleine-Weber, H., Schroeder, S., Krüger, N., Herrler, T., Erichsen, S., . . . Pöhlmann, S. (2020). SARS-CoV-2 Cell Entry Depends on ACE2 and TMPRSS2 and Is Blocked by a Clinically Proven Protease Inhibitor. *Cell*, *181*(2), 271-280.e278. https://doi.org/10.1016/j.cell.2020.02.052

Hogwood, J., Mulloy, B., Lever, R., Gray, E., & Page, C. P. (2023). Pharmacology of Heparin and Related Drugs: An Update. *Pharmacological Reviews*, *75*(2), 328-379. https://doi.org/10.1124/pharmrev.122.000684

Hsieh, C.-L., Goldsmith, J. A., Schaub, J. M., Divenere, A. M., Kuo, H.-C., Javanmardi, K., . . . Mclellan, J. S. (2020). Structure-based design of prefusion-stabilized SARS-CoV-2 spikes. *Science*, *369*(6510), 1501-1505. https://doi.org/10.1126/science.abd0826

Hsu, Y. P., Frank, M., Mukherjee, D., Shchurik, V., Makarov, A., & Mann, B. F. (2023). Structural remodeling of SARS-CoV-2 spike protein glycans reveals the regulatory

roles in receptor-binding affinity. *Glycobiology*, *33*(2), 126-137. https://doi.org/10.1093/glycob/cwac077

Huang, H.-C., Lai, Y.-J., Liao, C.-C., Wang, F.-Y., Huang, K.-B., Lee, I.-J., . . . Li, C.-W. (2021). Targeting conserved N-glycosylation blocks SARS-CoV-2 variant infection in vitro. *eBioMedicine*, *74*, 103712. https://doi.org/10.1016/j.ebiom.2021.103712

Humphrey, W., Dalke, A., & Schulten, K. (1996). VMD: visual molecular dynamics. *J Mol Graph*, *14*(1), 33-38, 27-38. https://doi.org/10.1016/0263-7855(96)00018-5

Kearns, F. L., Sandoval, D. R., Casalino, L., Clausen, T. M., Rosenfeld, M. A., Spliid, C. B., . . . Esko, J. D. (2022). Spike-heparan sulfate interactions in SARS-CoV-2 infection. *Current Opinion in Structural Biology*, *76*, 102439. https://doi.org/10.1016/j.sbi.2022.102439

Kim, S. H., Kearns, F. L., Rosenfeld, M. A., Casalino, L., Papanikolas, M. J., Simmerling, C., . . . Freeman, R. (2022). GlycoGrip: Cell Surface-Inspired Universal Sensor for Betacoronaviruses. *ACS Central Science*, *8*(1), 22-42. https://doi.org/10.1021/acscentsci.1c01080

Kim, S. H., Kearns, F. L., Rosenfeld, M. A., Votapka, L., Casalino, L., Papanikolas, M., . . . Freeman, R. (2023). SARS-CoV-2 evolved variants optimize binding to cellular glycocalyx. *Cell Rep Phys Sci*, *4*(4), 101346. https://doi.org/10.1016/j.xcrp.2023.101346

Kim, S. Y., Jin, W., Sood, A., Montgomery, D. W., Grant, O. C., Fuster, M. M., . . . Linhardt, R. J. (2020). Characterization of heparin and severe acute respiratory syndrome-related coronavirus 2 (SARS-CoV-2) spike glycoprotein binding interactions. *Antiviral Res*, *181*, 104873. https://doi.org/10.1016/j.antiviral.2020.104873

Kirschner, K. N., Yongye, A. B., Tschampel, S. M., González-Outeiriño, J., Daniels, C. R., Foley, B. L., & Woods, R. J. (2008). GLYCAM06: A generalizable biomolecular force field. Carbohydrates. *Journal of Computational Chemistry*, *29*(4), 622-655. https://doi.org/10.1002/jcc.20820

Kokh, D. B., Amaral, M., Bomke, J., Grädler, U., Musil, D., Buchstaller, H.-P., . . . Wade, R. C. (2018). Estimation of Drug-Target Residence Times by τ-Random Acceleration Molecular Dynamics Simulations. *Journal of Chemical Theory and Computation*, *14*(7), 3859-3869. https://doi.org/10.1021/acs.jctc.8b00230

Kokh, D. B., Doser, B., Richter, S., Ormersbach, F., Cheng, X., & Wade, R. C. (2020). A workflow for exploring ligand dissociation from a macromolecule: Efficient random acceleration molecular dynamics simulation and interaction fingerprint analysis of ligand trajectories. *The Journal of Chemical Physics*, *153*(12), 125102. https://doi.org/10.1063/5.0019088

Lan, J., Ge, J., Yu, J., Shan, S., Zhou, H., Fan, S., . . . Wang, X. (2020). Structure of the SARS-CoV-2 spike receptor-binding domain bound to the ACE2 receptor. *Nature*, *581*(7807), 215-220. https://doi.org/10.1038/s41586-020-2180-5

Li, H., Robertson, A. D., & Jensen, J. H. (2005). Very fast empirical prediction and rationalization of protein pKa values. *Proteins*, *61*(4), 704-721. https://doi.org/10.1002/prot.20660

Li, Q., Wu, J., Nie, J., Zhang, L., Hao, H., Liu, S., . . . Wang, Y. (2020). The Impact of Mutations in SARS-CoV-2 Spike on Viral Infectivity and Antigenicity. *Cell*, *182*(5), 1284-1294.e1289. https://doi.org/10.1016/j.cell.2020.07.012

Liu, L., Chopra, P., Li, X., Bouwman, K. M., Tompkins, S. M., Wolfert, M. A., . . . Boons, G.-J. (2021). Heparan Sulfate Proteoglycans as Attachment Factor for SARS-CoV-2. *ACS Central Science*, *7*(6), 1009-1018. https://doi.org/10.1021/acscentsci.1c00010

Low, J. S., Jerak, J., Tortorici, M. A., McCallum, M., Pinto, D., Cassotta, A., . . . Sallusto, F. (2022). ACE2-binding exposes the SARS-CoV-2 fusion peptide to broadly neutralizing coronavirus antibodies. *Science*, *377*(6607), 735-742. https://doi.org/10.1126/science.abq2679

Lu, M., Chamblee, M., Zhang, Y., Ye, C., Dravid, P., Park, J.-G., . . . Li, J. (2022). SARS-CoV-2 prefusion spike protein stabilized by six rather than two prolines is more potent for inducing antibodies that neutralize viral variants of concern. *Proceedings of the National Academy of Sciences*, *119*(35). https://doi.org/10.1073/pnas.2110105119

Maier, J. A., Martinez, C., Kasavajhala, K., Wickstrom, L., Hauser, K. E., & Simmerling, C. (2015). ff14SB: Improving the Accuracy of Protein Side Chain and Backbone Parameters from ff99SB. *Journal of Chemical Theory and Computation*, *11*(8), 3696-3713. https://doi.org/10.1021/acs.jctc.5b00255

Mehdipour, A. R., & Hummer, G. (2021). Dual nature of human ACE2 glycosylation in binding to SARS-CoV-2 spike. *Proceedings of the National Academy of Sciences*, *118*(19), e2100425118. https://doi.org/10.1073/pnas.2100425118

Meng, B., Datir, R., Choi, J., Bradley, J. R., Smith, K. G. C., Lee, J. H., . . . King, R. (2022). SARS-CoV-2 spike N-terminal domain modulates TMPRSS2-dependent viral entry and fusogenicity. *Cell Reports*, *40*(7), 111220. https://doi.org/10.1016/j.celrep.2022.111220

Mori, T., Jung, J., Kobayashi, C., Dokainish, H. M., Re, S., & Sugita, Y. (2021). Elucidation of interactions regulating conformational stability and dynamics of SARS-CoV-2 S-protein. *Biophysical Journal*, *120*(6), 1060-1071. https://doi.org/10.1016/j.bpj.2021.01.012

Mycroft-West, C. J., Su, D., Pagani, I., Rudd, T. R., Elli, S., Gandhi, N. S., . . . Skidmore, M. A. (2020). Heparin Inhibits Cellular Invasion by SARS-CoV-2: Structural Dependence of the Interaction of the Spike S1 Receptor-Binding Domain with Heparin. *Thrombosis and Haemostasis*, *120*(12), 1700-1715. https://doi.org/10.1055/s-0040-1721319

Nangarlia, A., Hassen, F. F., Canziani, G., Bandi, P., Talukder, C., Zhang, F., . . . Chaiken, I. (2023). Irreversible Inactivation of SARS-CoV-2 by Lectin Engagement with Two Glycan Clusters on the Spike Protein. *Biochemistry*, *62*(14), 2115-2127. https://doi.org/10.1021/acs.biochem.3c00109

Newby, M. L., Fogarty, C. A., Allen, J. D., Butler, J., Fadda, E., & Crispin, M. (2023). Variations within the Glycan Shield of SARS-CoV-2 Impact Viral Spike Dynamics. *J Mol Biol*, *435*(4), 167928. https://doi.org/10.1016/j.jmb.2022.167928

Paiardi, G., Richter, S., Oreste, P., Urbinati, C., Rusnati, M., & Wade, R. C. (2022). The binding of heparin to spike glycoprotein inhibits SARS-CoV-2 infection by three mechanisms. *Journal of Biological Chemistry*, *298*(2), 101507. https://doi.org/10.1016/j.jbc.2021.101507

Parrinello, M., Rahman, & A. (1981). Polymorphic transitions in single crystals: A new molecular dynamics method. In (Vol. 52, pp. 7182–7190): *Journal of Applied Physics*.

Pekka, M., & Lennart, N. (2001). Structure and Dynamics of the TIP3P, SPC, and SPC/E Water Models at 298 K. *The Journal of Physical Chemistry A*, *105*(43), 9954-9960. https://doi.org/10.1021/jp003020w

Qing, E., Kicmal, T., Kumar, B., Hawkins, G. M., Timm, E., Perlman, S., & Gallagher, T. (2021). Dynamics of SARS-CoV-2 Spike Proteins in Cell Entry: Control Elements in the Amino-Terminal Domains. *mBio*, *12*(4), e0159021. https://doi.org/10.1128/mBio.01590-21

Qing, E., Li, P., Cooper, L., Schulz, S., Jäck, H. M., Rong, L., . . . Gallagher, T. (2022). Inter-domain communication in SARS-CoV-2 spike proteins controls protease-triggered cell entry. *Cell Rep*, *39*(5), 110786. https://doi.org/10.1016/j.celrep.2022.110786

Roe, D. R., & Cheatham, T. E. (2013). PTRAJ and CPPTRAJ: Software for Processing and Analysis of Molecular Dynamics Trajectory Data. *J Chem Theory Comput*, *9*(7), 3084-3095. https://doi.org/10.1021/ct400341p

Shang, J., Ye, G., Shi, K., Wan, Y., Luo, C., Aihara, H., . . . Li, F. (2020). Structural basis of receptor recognition by SARS-CoV-2. *Nature*, *581*(7807), 221-224. https://doi.org/10.1038/s41586-020-2179-y

Shin, Y. H., Jeong, K., Lee, J., Lee, H. J., Yim, J., Kim, J., . . . Park, S. B. (2022). Inhibition of ACE2-Spike Interaction by an ACE2 Binder Suppresses SARS-CoV-2 Entry. *Angewandte Chemie International Edition*, *61*(11). https://doi.org/10.1002/anie.202115695

Sousa Da Silva, A. W., & Vranken, W. F. (2012). ACPYPE - AnteChamber PYthon Parser interfacE. *BMC Research Notes*, *5*(1), 367. https://doi.org/10.1186/1756-0500-5-367

Spinello, A., Saltalamacchia, A., & Magistrato, A. (2020). Is the Rigidity of SARS-CoV-2 Spike Receptor-Binding Motif the Hallmark for Its Enhanced Infectivity? Insights from All-Atom Simulations. *The Journal of Physical Chemistry Letters*, *11*(12), 4785-4790. https://doi.org/10.1021/acs.jpclett.0c01148

Sun, L., Chopra, P., Tomris, I., Van Der Woude, R., Liu, L., De Vries, R. P., & Boons, G.-J. (2023). Well-Defined Heparin Mimetics Can Inhibit Binding of the Trimeric Spike of SARS-CoV-2 in a Length-Dependent Manner. *JACS Au*, *3*(4), 1185-1195. https://doi.org/10.1021/jacsau.3c00042

Sztain, T., Ahn, S.-H., Bogetti, A. T., Casalino, L., Goldsmith, J. A., Seitz, E., . . . Amaro, R. E. (2021). A glycan gate controls opening of the SARS-CoV-2 spike protein. *Nature Chemistry*, *13*(10), 963-968. https://doi.org/10.1038/s41557-021-00758-3

Tree, J. A., Turnbull, J. E., Buttigieg, K. R., Elmore, M. J., Coombes, N., Hogwood, J., . . . Carroll, M. W. (2021). Unfractionated heparin inhibits live wild type SARS-CoV-2 cell infectivity at therapeutically relevant concentrations. *British Journal of Pharmacology*, *178*(3), 626-635. https://doi.org/10.1111/bph.15304

Van Der Spoel, D., Lindahl, E., Hess, B., Groenhof, G., Mark, A. E., & Berendsen, H. J. (2005). GROMACS: fast, flexible, and free. *J Comput Chem*, *26*(16), 1701-1718. https://doi.org/10.1002/jcc.20291

Vankadari, N., Ketavarapu, V., Mitnala, S., Vishnubotla, R., Reddy, D. N., & Ghosal, D. (2022). Structure of Human TMPRSS2 in Complex with SARS-CoV-2 Spike Glycoprotein and Implications for Potential Therapeutics. *The Journal of Physical Chemistry Letters*, *13*(23), 5324-5333. https://doi.org/10.1021/acs.jpclett.2c00967

Verkhivker, G., Alshahrani, M., Gupta, G., Xiao, S., & Tao, P. (2023). *Probing Conformational Landscapes of Binding and Allostery in the SARS-CoV-2 Omicron Variant Complexes Using Microsecond Atomistic Simulations and Perturbation-Based Profiling Approaches: Hidden Role of Omicron Mutations as Modulators of Allosteric Signal*. Cold Spring Harbor Laboratory.

Walls, A. C., Park, Y.-J., Tortorici, M. A., Wall, A., Mcguire, A. T., & Veesler, D. (2020). Structure, Function, and Antigenicity of the SARS-CoV-2 Spike Glycoprotein. *Cell*, *181*(2), 281-292.e286. https://doi.org/10.1016/j.cell.2020.02.058

Wang, J., Wolf, R. M., Caldwell, J. W., Kollman, P. A., & Case, D. A. (2004). Development and testing of a general amber force field. *J Comput Chem*, *25*(9), 1157-1174. https://doi.org/10.1002/jcc.20035

Wang, Q., Zhang, Y., Wu, L., Niu, S., Song, C., Zhang, Z., . . . Qi, J. (2020). Structural and Functional Basis of SARS-CoV-2 Entry by Using Human ACE2. *Cell*, *181*(4), 894-904.e899. https://doi.org/10.1016/j.cell.2020.03.045

Watanabe, Y., Allen, J. D., Wrapp, D., McLellan, J. S., & Crispin, M. (2020). Site-specific glycan analysis of the SARS-CoV-2 spike. *Science*, *369*(6501), 330-333. https://doi.org/10.1126/science.abb9983

Williams, J. K., Wang, B., Sam, A., Hoop, C. L., Case, D. A., & Baum, J. (2022). Molecular dynamics analysis of a flexible loop at the binding interface of the SARS-CoV-2 spike protein receptor-binding domain. *Proteins: Structure, Function, and Bioinformatics*, *90*(5), 1044-1053. https://doi.org/10.1002/prot.26208

Xie, Y., & Butler, M. (2023). Quantitative profiling of N-glycosylation of SARS-CoV-2 spike protein variants. *Glycobiology*, *33*(3), 188-202. https://doi.org/10.1093/glycob/cwad007

Xu, C., Wang, Y., Liu, C., Zhang, C., Han, W., Hong, X., . . . Cong, Y. (2021). Conformational dynamics of SARS-CoV-2 trimeric spike glycoprotein in complex with receptor ACE2 revealed by cryo-EM. *Sci Adv*, *7*(1). https://doi.org/10.1126/sciadv.abe5575

Yang, J., Petitjean, S. J. L., Koehler, M., Zhang, Q., Dumitru, A. C., Chen, W., . . . Alsteens, D. (2020). Molecular interaction and inhibition of SARS-CoV-2 binding to the ACE2 receptor. *Nature Communications*, *11*(1). https://doi.org/10.1038/s41467-020-18319-6

Yang, Q., Hughes, T. A., Kelkar, A., Yu, X., Cheng, K., Park, S., . . . Neelamegham, S. (2020). Inhibition of SARS-CoV-2 viral entry upon blocking N- and O-glycan elaboration. *Elife*, *9*. https://doi.org/10.7554/eLife.61552

Yang, Q., Kelkar, A., Sriram, A., Hombu, R., Hughes, T. A., & Neelamegham, S. (2022). Role for N-glycans and calnexin-calreticulin chaperones in SARS-CoV-2 Spike maturation and viral infectivity. *Science Advances*, *8*(38). https://doi.org/10.1126/sciadv.abq8678

Yang, Y., Du, Y., & Kaltashov, I. A. (2020). The Utility of Native MS for Understanding the Mechanism of Action of Repurposed Therapeutics in COVID-19: Heparin as a Disruptor of the SARS-CoV-2 Interaction with Its Host Cell Receptor. *Analytical Chemistry*, *92*(16), 10930-10934. https://doi.org/10.1021/acs.analchem.0c02449

Yu, S., Zheng, X., Zhou, B., Li, J., Chen, M., Deng, R., . . . Meng, G. (2022). SARS-CoV-2 spike engagement of ACE2 primes S2' site cleavage and fusion initiation. *Proc Natl Acad Sci U S A*, *119*(1). https://doi.org/10.1073/pnas.2111199119

Yuan, M., Wu, N. C., Zhu, X., Lee, C. D., So, R. T. Y., Lv, H., . . . Wilson, I. A. (2020). A highly conserved cryptic epitope in the receptor binding domains of SARS-CoV-2 and SARS-CoV. *Science*, *368*(6491), 630-633. https://doi.org/10.1126/science.abb7269

Zhao, P., Praissman, J. L., Grant, O. C., Cai, Y., Xiao, T., Rosenbalm, K. E., . . . Wells, L. (2020). Virus-Receptor Interactions of Glycosylated SARS-CoV-2 Spike and Human ACE2 Receptor. *Cell Host & Microbe*, *28*(4), 586-601.e586. https://doi.org/10.1016/j.chom.2020.08.004

Zheng, L., Ma, Y., Chen, M., Wu, G., Yan, C., & Zhang, X. E. (2021). SARS-CoV-2 spike protein receptor-binding domain N-glycans facilitate viral internalization in respiratory

epithelial cells. *Biochem Biophys Res Commun*, *579*, 69-75. https://doi.org/10.1016/j.bbrc.2021.09.053

Zhu, R., Canena, D., Sikora, M., Klausberger, M., Seferovic, H., Mehdipour, A. R., . . . Hinterdorfer, P. (2022). Force-tuned avidity of spike variant-ACE2 interactions viewed on the single-molecule level. *Nat Commun*, *13*(1), 7926. https://doi.org/10.1038/s41467-022-35641-3